

Supporting Information

Meter-scale chemiluminescent carbon nanodot films for temperature imaging†

Guang-Song Zheng,^{ab} Cheng-Long Shen,^{ab} Qing Lou,^{*a} Jiang-Fan Han,^a Zhong-Zheng Ding,^a Yuan Deng,^a Meng-Yuan Wu,^a Kai-Kai Liu,^a Jin-Hao Zang,^a Lin Dong^a and Chong-Xin Shan^{*a}

Methods

Synthesize of efficient fluorescent CDs. In this work, the CDs were synthesized with solvothermal treatment of CA and OPD. In detail, 0.1-g CA and 0.1-g OPD were dispersed in the mixed solution of 10-mL deionized water and 10-mL DMF. Then the mixtures were transferred into the Teflon-lined stainless autoclave (20 mL) and the sealed autoclave vessels were placed into an electric oven. After treated at 200 °C for 10 h, the obtained solvents were purified via silica column chromatography with dichloromethane (CH₂Cl₂) as eluent. The bright yellow fluorescent CDs under 365 nm UV lamp were obtained and further collected by vacuum drying at 60 °C for 1 day.

The calculation of CL QY. The CL QYs of the CDs were measured using lucigenin with H₂O₂ as oxidant with a known QY of 8.3×10⁻³ einsteins mol⁻¹ at pH = 11 according to the previous literatures. According to the CL spectra and kinetic curves, the CL QYs were calculated according to the following equations:

$$\phi_{CL} = \frac{Q \times f_{luc} \times f_{photo}}{n} \text{ (einsteins / mol)} \quad (1)$$

$$f_{luc} = \frac{\phi_{luc} \times n_{luc}}{Q_{luc}} \quad (2)$$

$$f_{photo} = \frac{f(\lambda_s)}{f(\lambda_{luc})} \quad (3)$$

Where ϕ_{CL} is the CL QYs of CDs, Q is the total light emission obtained by integration of emission intensity under time curves. f_{luc} is obtained by measuring the emission kinetics of lucigenin reaction performed in standard conditions. f_{photo} is obtained from the sensitivity at the emission wavelength (λ_{max} = 475 nm) of the lucigenin standard, $f(\lambda_{luc})$, and the emission of the CDs, $f(\lambda_s)$. n is the number of moles of lucigenin (n_{luc}) or the number of moles of CPPO.

Preparation of CD-based CL films. Herein, 4-g F127 were homogeneously dispersed into 40-mL CH₂Cl₂ solution. Then 10-ml CDs CH₂Cl₂ solution (3 mg ml⁻¹) and 0.2-g CPPO were added into the F127 colloid solution. After stirring for 20 min, the obtained solution was used to prepare the film with the scraping process.

Temperature-responsive CL emission of films. The time-dependent CL spectra and illumination intensity induced by the CDs was recorded with the collection of F-7000 and luminance meter, respectively. For the temperature-responsive CL emission, the films kept on the heating stage with different temperature were recorded in 10 s after spraying the H₂O₂ solution by the F-7000 and luminance meter, respectively.

CL imaging for accurate temperature measurement. Herein, the CL imaging was achieved with a common mobile phone and a personal software for relationship between the CL intensity and temperature was edited with the data handled with MATLAB. In detail, the common CL photography of the film after spraying the H₂O₂ solution were recorded by the common mobile phone. With the treatment of MATLAB, the relationship between the CL intensity and temperature was established with the corresponding gray level from the photograph. With the relationship, the photography with the distribution of CL intensity could be translated to the corresponding temperature distribution, enabling the CL imaging and accurate temperature measurement.

Method of temperature imaging by the CL film using mobile phone. Firstly, under the same parameters, the CL photos under different temperatures are taken. And the gray values of the photos are obtained by Matlab processing. The average value of the values is taken as the standard card data, as shown in the Fig S8. And the relationship between the gray level of the photos and the temperature is obtained by data fitting. Then, this algorithm is written into the mobile phone app, which can complete the processing of the CL photos on the mobile phone and obtain the temperature distribution information.

Characterizations. The morphology and structure were captured by an AIST-NT Smart atomic force microscope (AFM), JSM-6700F scanning electron microscope (SEM), JEOL-2010 transmission electron microscopy (TEM), and a Bruker-D8 Discover X-ray

diffractometer (XRD) with the Cu K α line ($\lambda = 1.54 \text{ \AA}$) as the irradiation source. The X-ray photoelectron spectroscopy (XPS) was evaluated on a Kratos AXIS HIS 165 spectrometer with a monochromatized Al KR X-ray source (1486.7 eV). Fourier transform infrared spectroscopy (FTIR) was measured by a Thermo Scientific Nicolet iZ 10 spectrometer in the KBr tablets. The ^1H and ^{13}C chemical shift were probed by Bruker 400/600M AVANCEIII nuclear magnetic resonance (NMR) in CDCl. Photograph was obtained from a HUAWEI mobile phone (HUAWEI CLT-AL01, China). The fluorescence and chemiluminescence spectrum and luminance were measured by a Hitachi F-7000 spectrofluorometer and a LS-160 luminance meter (Konica Minolta). The absorption spectrum was obtained by an UV/VIS spectrophotometer (Hitachi, UH-4150). The fluorescence decay curves were gained by Horiba FL-322 using a 370 nm Nano-LED monitoring the related emission. The PL QY was measured by the spectrophotometer (FLS1000) with an integrating sphere test system. Transient absorption spectra were acquired by a home-built ultra-fast measurement system with an 800-nm femtosecond seed light as a source of light. The mechanical performance of the films was measured by a universal testing machine (Mark-10). Thermal imaging was also got from a commercial infrared camera (FLIR) for comparison.

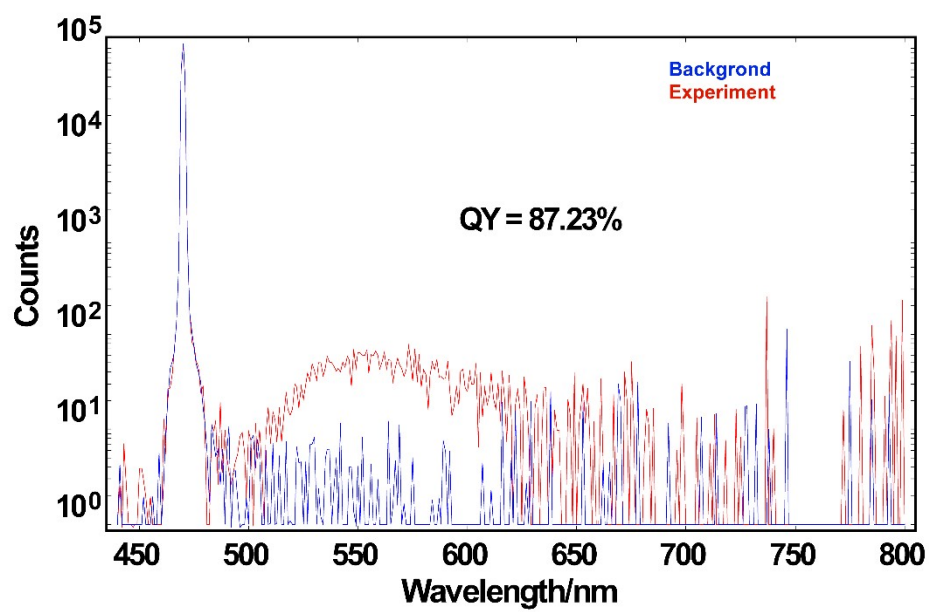


Figure S1. Calculation of the fluorescence quantum yield of the CDs.

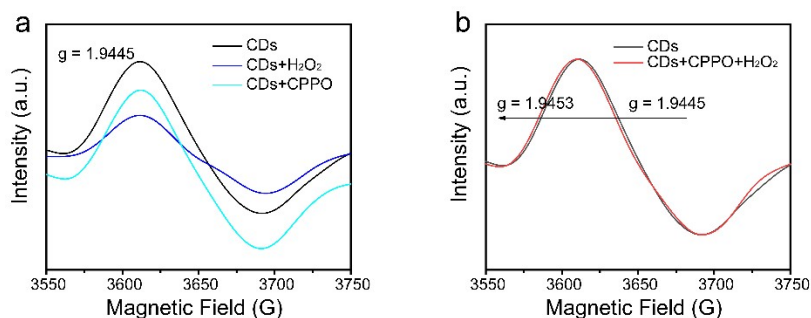


Figure S2. (a) ESR spectra of the CDs, CDs/CPPO, and CDs/H₂O₂. (b) ESR spectra of the CDs before and after the addition of H₂O₂ and CPPO.

Note: In addition, electron spin resonance (ESR) method was also used to investigate the ground-state properties of luminescent species in the CDs. As shown in Figure S2a, the CDs show ESR signal at $g = 1.9445$, which illustrates singly occupied orbit in the ground state of the CDs. The singly occupied orbit indicates that the CDs can act as electron donors or acceptors during the CL process. The g -value of the CDs after their reaction with CPPO or H₂O₂ shows little shift compared to that of the pristine CDs, which verifies that there is no direct interaction between CDs and CPPO or H₂O₂. Moreover, the g -value of the CDs increases from 1.9445 to 1.9453 after the simultaneous addition of H₂O₂ and CPPO, indicating electron exchange between the singly occupied orbit in the CDs and intermediate during the CL process (Figure S2b). Hence, electron transfer from CDs to the intermediate indeed exists in the CL process and the CL of the CDs is the only consequence of the direct chemical electron exchange between 1,2-dioxetanedione (intermediate) and the CDs.

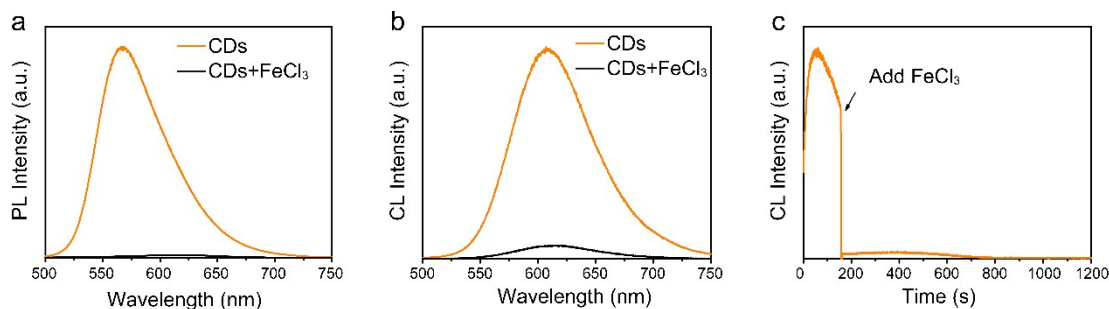


Figure S3. (a) PL spectra of CDs before and after adding Fe^{3+} . (b) CL spectra of CDs before and after adding Fe^{3+} . (c) CL intensity decay of CDs after the addition of Fe^{3+} .

Note: For the electron exchange between 1,2-dioxetanedione (intermediate) and the CDs in the CL, the electron exchange luminescence has been supported by the Stern-Volmer quenching analysis, which is measured by the time-resolved decay spectra (Figure S3). Fe^{3+} , as an efficient PL quenching agent, has been extensively investigated as an electron acceptor in luminescence systems. As shown in Figure S3a, the CDs show a typical PL quenching after the addition of Fe^{3+} , which proves the electron transfer from the CDs to Fe^{3+} . Similarly, the CL of the CDs can be also quenched by Fe^{3+} . As shown in Figures S3b and S3c, the addition of Fe^{3+} in the CDs-CPPO- H_2O_2 CL system can decrease the CL intensity sharply, which means that the electron transfer from the CDs to the energetic intermediate during the CL process can be captured by the stronger electron trapping agent of Fe^{3+} .

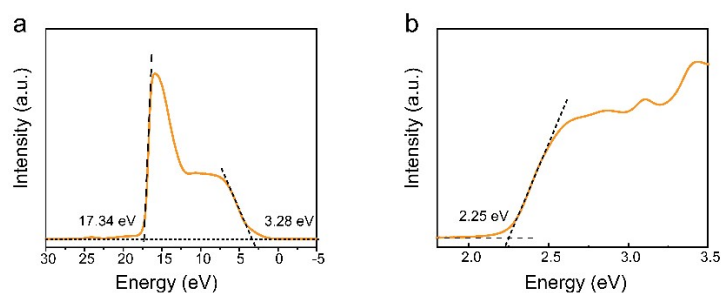


Figure S4. The energy level distribution of CDs was calculated with the (a) ultraviolet photoelectron spectroscopy (UPS) and (b) optical absorption spectra.

Note: The HOMO/LUMO levels of the CDs have been defined by ultraviolet photoelectron spectroscopy (UPS). As shown in the Figure S4a, the cutoff region of the CDs was 17.34 eV, and the LUMO level of CDs was further calculated to be ~ 7.16 eV according to the equation: $E_{\text{LUMO}} = 21.22 - E_{\text{cutoff region}} + E_{\text{valence region}}$. Combined with the bandgap energy of CDs (2.25 eV) obtained from the Tauc-plot fitted curves derived from optical absorption spectra (Figure S4b), we can obtain the HOMO level of CDs as 4.91 eV based on the $E_{\text{HOMO}} = E_{\text{LUMO}} - E_{\text{gap}}$. The LUMO of 1,2-dioxetanedione was 3.2 eV close to the HOMO level of CDs (4.91 eV), which is beneficial to the electron exchange between the energetic intermediate produced in the CL reaction (1,2-dioxetanedione) and the CDs.

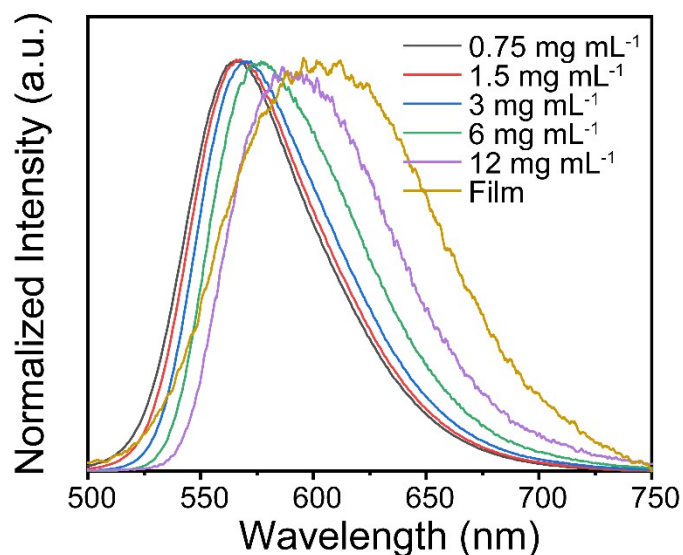


Figure S5. Normalized fluorescence spectra of CDs with different concentration.

Note: Indeed, the emission of CDs is beyond 600 nm after spraying H_2O_2 solution onto the CD film, which is a little different from that of 580 nm in solution (Figure 2b). The significant difference can be attributed to the concentration-induced spectral shift of CDs. For the CD solid film, the concentration of CDs is higher in comparison with the CDs in toluene solution. As shown in Figure S5, with the increase of the concentration in CD solution until it becomes a solid film, the spectra of the CDs gradually shift from 576 nm to 615 nm under 365-nm light excitation. This red-shift process originates from the aggregation-induced resonance energy transfer between the CDs in high-concentration solution or solid state. Thus, because of the efficient energy transfer, the short wavelength of emission that overlaps the absorption of the CDs can be effectively weakened, whereas the long wavelength is comparatively strengthened. This phenomenon is consistent with the previous report (Adv. Mater., 2016, 28, 312-318).

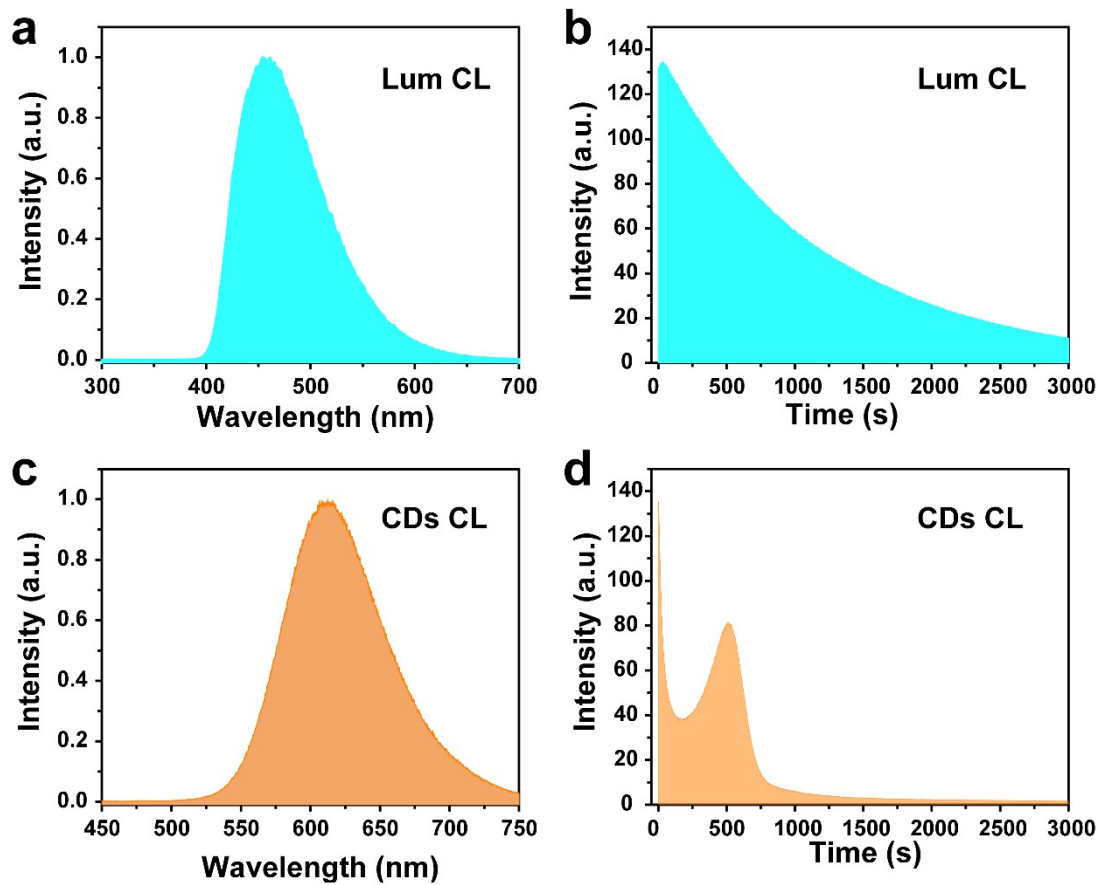


Figure S6. Calculation of the CL quantum yield of the CDs.

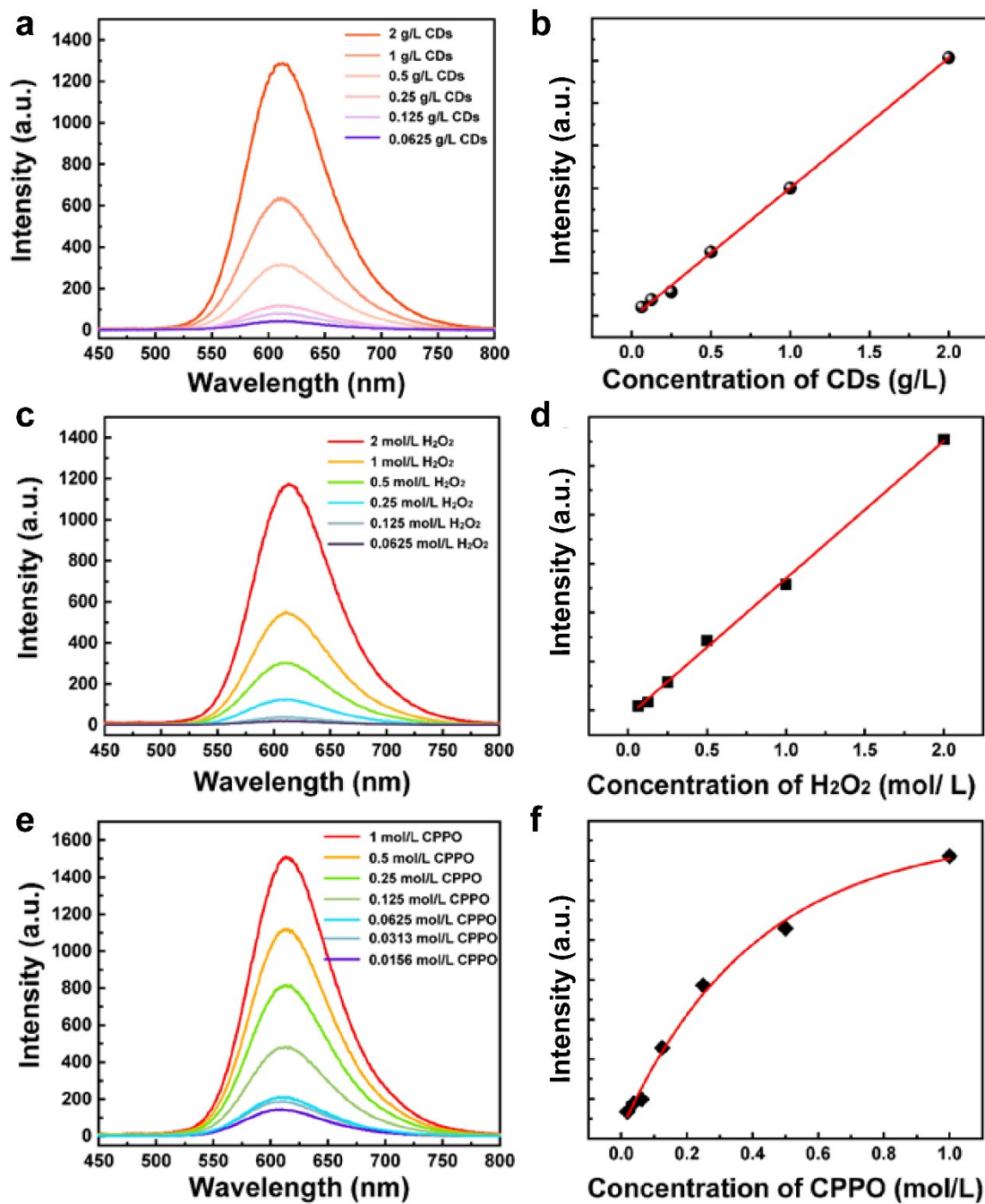


Figure S7. CL spectra and integral intensity with the different concentration of CDs (a, b), hydrogen peroxide (c, d) and CPPO (e, f)

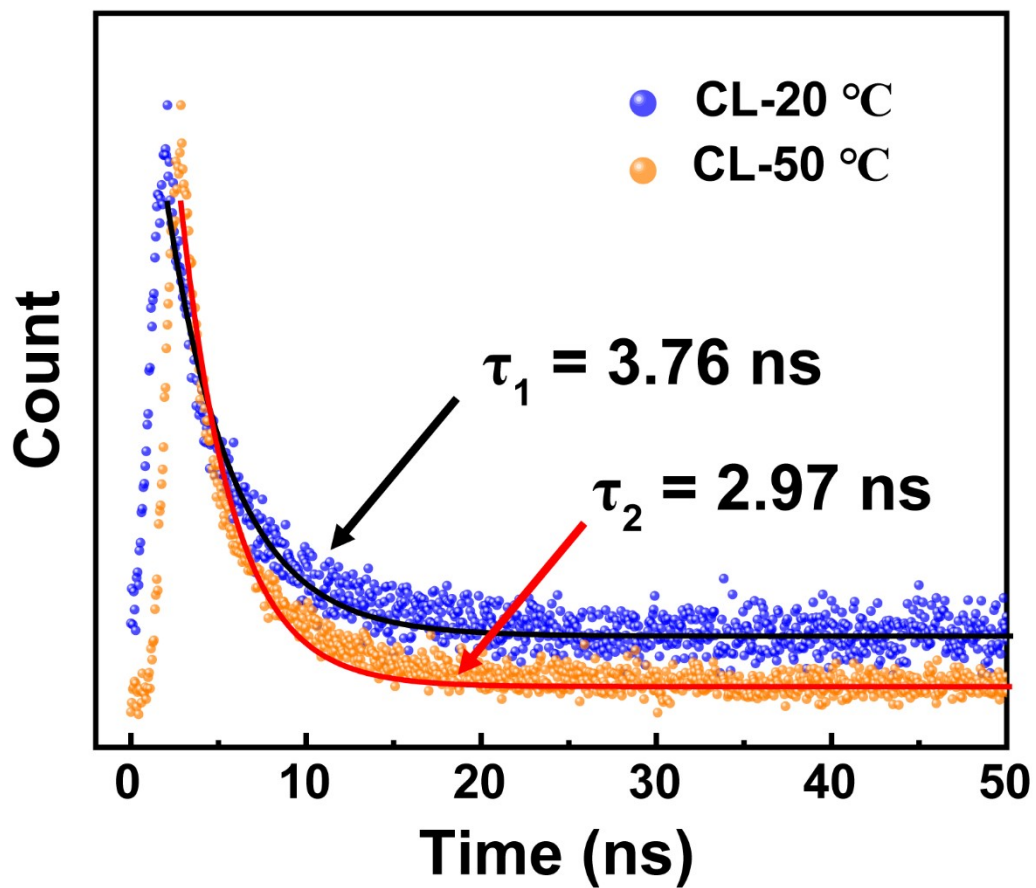


Figure S8. Time-resolved decay spectra of CL CLs under different temperature.

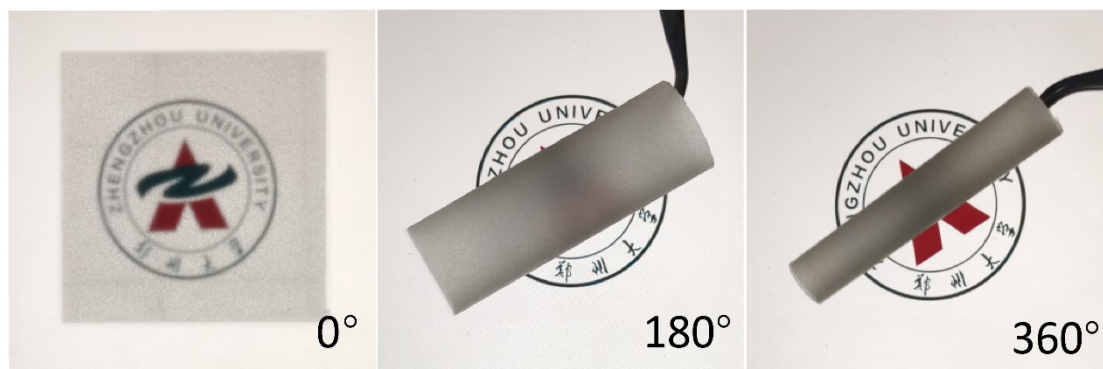


Figure S9. Photos of CD-based CL films under different bending degrees.

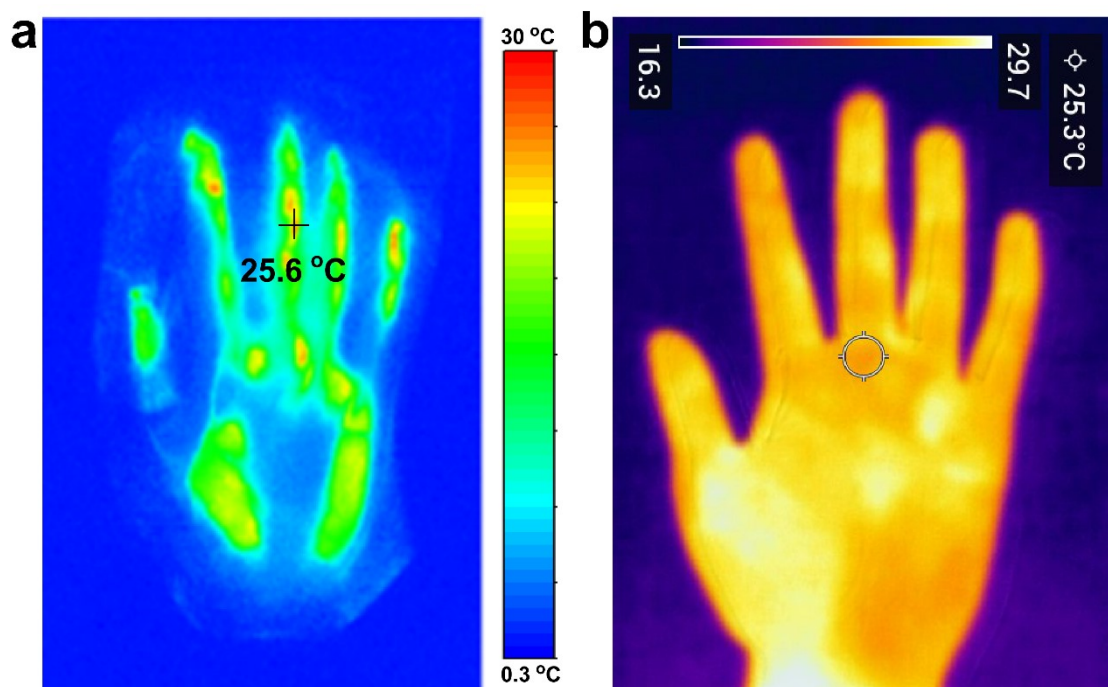


Figure S10. Comparison of palm thermal imaging with CD-based CL film a) and commercial infrared cameras b).

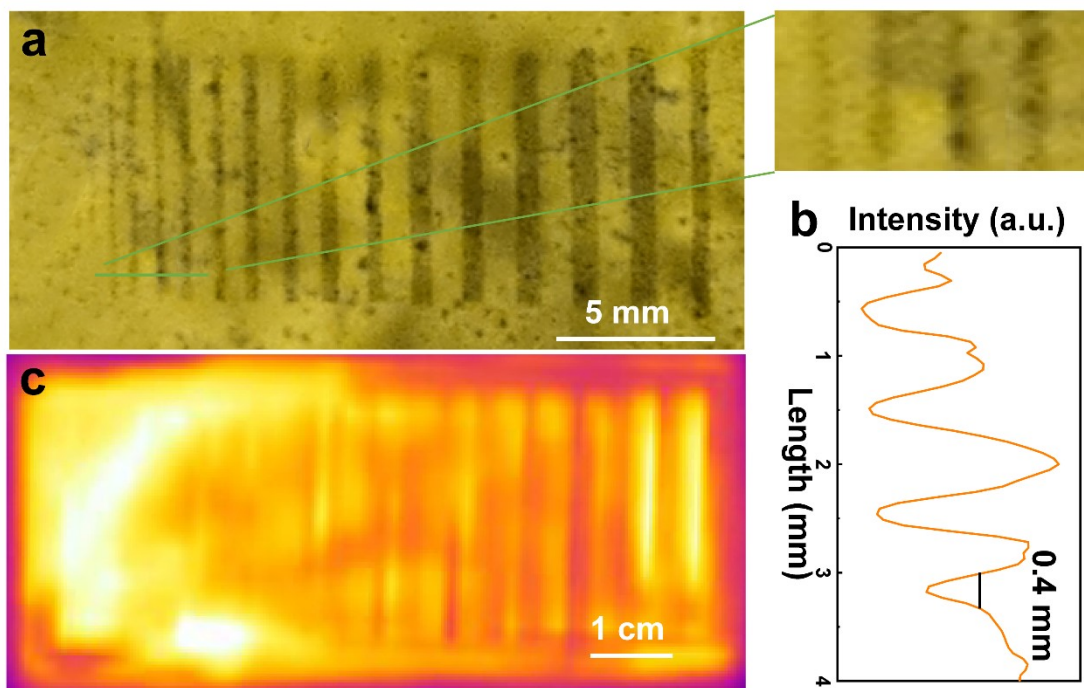


Figure S11. Spatial resolution test. a) Temperature imaging with CL film. b) Intensity curve of CD-based CL film thermal imaging. c) Temperature imaging with commercial infrared camera. (The hot metal background is about 50 °C).

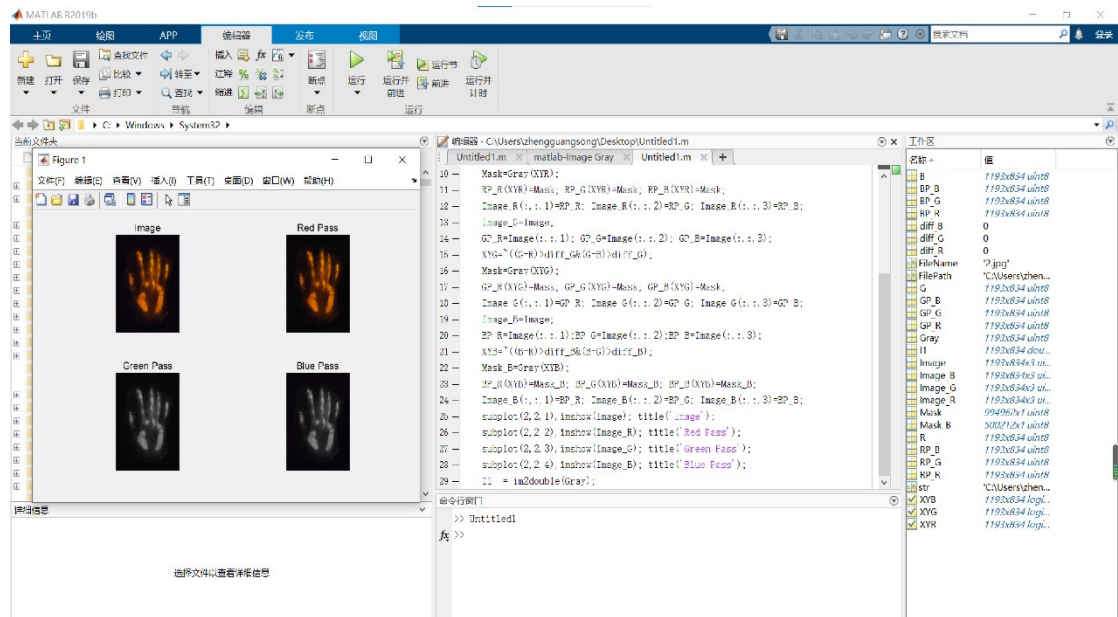


Figure S12. Screenshot of palm CL temperature imaging processed by MATLAB.

Table S1. The sensitivity and range of various nano-thermometers for temperature detecting.

Temperature sensing systems	Materials	Temperature measuring range (K)	temperature specific sensitivity	References
PL Intensity	Ruphen	280–315	0.0114	1
	Rhodamine-B	287–363	0.0267	2
	CdSe/ZnS	278–313	0.025	3
	NV NDs	295–400	0.01	4
PL ratio	Bis(pyrene) propane	310–465	0.256	5
	Zn ₁ –Mn _x Se/ZnCdSe	134–400	0.07	6
	Er ³⁺ /Yb ³⁺ CaF ₂	293–318	0.02	7
	Tm ³⁺ /Yb ³⁺ CaF ₂	293–318	0.002	7
	NaYF ₄ :Er ³⁺ , Yb ³⁺	298–334	0.0116	8
	NaLuF ₄ :Yb, Er	273–348	0.011	9
	ZnO:Er ³⁺	278–463	0.011	10
	β-NaYF ₄ :20%Yb2%Er	294–334	0.0164	11
Wavelength shift	(Gd,Yb,Er) ₂ O ₃	300–1050	0.017	12
	Triarylboron	223–373	0.0078	13
	CdSe	293–323	0.000161	14
PL lifetime	CdSe/ZnS	284–320	0.000268	15
	CdTe	293–333	0.011	16
	Eu-doped complex	273-343	0.020	17
	Au nanocluster	288-318	0.013	18
	perovskites	173-383	0.06	19
	Poly(DBD-AE-co-NOPAM)	296-313	0.060	20
CL	CDs	288-328	0.08	This work

Reference

1. Muhammet Erkan Koşse, Bruce F. Carroll, a. K. S. Schanze, *Langmuir*, 2005, **21**, 9121-9129.
2. M. G. David Ross, and Laurie E. Locascio, *Anal. Chem.*, 2001, **73**, 4117-4123.
3. G. W. Walker, V. C. Sundar, C. M. Rudzinski, A. W. Wun, M. G. Bawendi, D. G. Nocera, *Appl. Phys. Lett.*, 2003, **83**, 3555-3557.
4. T. Plakhotnik, H. Aman, H. C. Chang, *Nanotechnology*, 2015, **26**, 2c501.

5. K. B. M. a. A. J. BUR, *Polym. Eng. Sci.*, 1998, **38**, 213-221.
6. V. A. Vlaskin, N. Janssen, J. van Rijssel, R. Beaulac, D. R. Gamelin, *Nano Lett.*, 2010, **10**, 3670-3674.
7. O. A. Savchuk, P. Haro-Gonzalez, J. J. Carvajal, D. Jaque, J. Massons, M. Aguilo, F. Diaz, *Nanoscale*, 2014, **6**, 9727-9733.
8. R. N. Fiorenzo Vetrone, Alicia Zamarró'n, Angeles Juarranz de la Fuente, Francisco Sanz-Rodríguez, Laura Martínez Maestro, Emma Martí'n Rodríguez, Daniel Jaque, José' Garcí'aSole', John A. Capobianco, *ACS Nano*, 2010, **4**, 3254-3258.
9. X. Zhu, W. Feng, J. Chang, Y. W. Tan, J. Li, M. Chen, Y. Sun, F. Li, *Nat. Commun.*, 2016, **7**, 10437.
10. X. K. Xin Wang, Yi Yu, Yajuan Sun, Hong Zhang, *J. Phys. Chem. C*, 2007, **111**, 15119-15124.
11. K. Green, K. Huang, H. Pan, G. Han, S. F. Lim, *Front. Chem.*, 2018, **6**, 416.
12. D. A. Mengistie L. Debasu, Isabel Pastoriza-Santos, Luis M. Liz-Marzán, J. Rocha, Luis D. Carlos, *Adv. Mater.*, 2013, **23**, 4817.
13. J. Feng, K. Tian, D. Hu, S. Wang, S. Li, Y. Zeng, Y. Li, G. Yang, *Angew. Chem. Int. Ed. Engl.*, 2011, **50**, 8072-8076.
14. K. Z. Sha Li, Jui-Ming Yang, Liwei Lin, Haw Yang, *Nano Lett.*, 2007, **7**, 3102-3105.
15. M. A. M. Pedro Jorge, Tito Trindade, José Luís Santos, Faramarz Farahi, *Sensors*, 2007, **7**, 3489-3534.
16. P. Haro-Gonzalez, L. Martínez-Maestro, I. R. Martín, J. García-Sole, D. Jaque, *Small*, 2012, **8**, 2652-2658.
17. J. Yu, L. Sun, H. Peng, M. I. J. Stich, *J. Mater. Chem.*, 2010, **20**, 6975-6981.
18. L. Shang, F. Stockmar, N. Azadfar, G. U. Nienhaus, *Angew. Chem. Int. Ed. Engl.*, 2013, **52**, 11154-11157.
19. S. Yakunin, B. M. Benin, Y. Shynkarenko, O. Nazarenko, M. I. Bodnarchuk, D. N. Dirin, C. Hofer, S. Cattaneo, M. V. Kovalenko, *Nat. Mater.*, 2019, **18**, 846-852.
20. E. M. Graham, K. Iwai, S. Uchiyama, A. P. de Silva, S. W. Magennis, A. C. Jones, *Lab. Chip.*, 2010, **10**, 1267-1273.